Communication

Investigation of Deformation Mechanisms in β-Type Ti-35Nb-2Ta-3Zr Alloy *via* FSP Leading to Surface Strengthening

LIQIANG WANG, JIAO QU, LIANGYU CHEN, QIANG MENG, LAI-CHANG ZHANG, JINING QIN, DI ZHANG, and WEIJIE LU

Friction-stir processing (FSP) is used to prepare Ti-35Nb-2Ta-3Zr alloys *via* different processing routes. Dislocation walls and tangles, deformation-induced α'' martensite, and deformation-induced ω phase are observed. The dominant deformation mechanisms are altered from deformation-induced α'' martensitic transformation and dislocation walls to twinning upon increasing the FSP passes. A reverse deformation-induced ω to β transformation and de-twinning process are observed together with grain refinement to the nanoscale. Meanwhile, compressive distortions along [0001]ω direction are favorable for the transformation from ω to β.

DOI: 10.1007/s11661-015-3089-8

As a unique deformation mechanism *via* shear bands (giant faults) without dislocation motion was observed in Ti-Nb-Ta-Zr-O alloy several years ago,[1] more investigations have been focusing on the deformation behavior of β titanium alloys.[2,3] Recently, systematic studies on Ti-Nb-Ta-Zr β titanium alloys have also been reported particularly with regard to the microstructural evolution and deformation mechanisms processed by cold rolling, warm swaging, or warm rolling.[4–6] Hao *et al.*[7] has found grain refinement to the nanoscale in the Ti-24Nb-4Zr-8Sn alloy after swaging and warm rolling. Wang *et al.*[8] have investigated deformation behavior in Ti-35Nb-2Ta-3Zr alloy during cold rolling (CR) and found that the dominant deformation mechanism is altered from stress-induced α'' martensitic transformation and twinning to dislocation slipping with the increasingCR reduction. Similar results were also obtained by Xu *et al.* in cold-deformed Ti-Nb-Ta-Zr-Fe alloy.[9] Wang *et al.*[10] found that during high-pressure torsion processing, a reverse ω to β transformation is observed when the grains are refined to the nanoscale in Ti-36Nb-2.2Ta-3.7Zr-0.3O alloy. Accompanying the complex deformation mechanisms, grain refinement is generally attributed to dislocation activity such as dislocation multiplication and interaction.[11–15] For materials with low stacking fault energies (SFEs), grains can be significantly refined by a combination of deformation twinning[8,16] and stress-induced phase transformation.[17–19] Except for commonly observed stress-induced α'' martensitic transformation, deformation-induced ω phase transformation is also obtained in β titanium alloys, which is expected to occur during cold-working processes.[20] More recently, a new solid-state surface modification technique, friction-stir processing (FSP) was developed for microstructural modification, which significantly refined grains to optimize surface properties.[21] However, little work regarding FSPed β-type titanium alloy and the associated deformation mechanisms is available. Despite these previous studies, the deformation mechanism combined with α'' and ω phases transformation is still not yet well understood, especially for the surface-modified β titanium alloy *via* severe plastic deformation. Furthermore, the experimental evidence for interaction mechanism of dislocations, twinning, deformation-induced α'' and ω phases has not yet been addressed in detail. In the current study, FSP method was adopted to process the Ti-35Nb-2Ta-3Zr β titanium alloy with the aim to investigate the deformation mechanisms.

The quaternary alloy with a nominal composition of Ti-35Nb-2Ta-3Zr (in wt pct) was prepared by arc melting the mixture of high-purity sponge titanium, Ti-Nb interalloy, Ta, and Zr. The ingot was re-melted three times for chemical homogeneity. The as-cast ingot was homogenized at 1223 K (950 °C) for 3.6 ks in vacuum condition and then forged into a billet of 40 mm in diameter and 160 mm in length, followed by a solution treatment at 1053 K (780 °C) for 1.8 ks by air cooling. FSP was performed at a rotational speed of 375 rpm and a traverse speed of 50 mm/min. The traverse direction was parallel to the plate's rolling direction. Three FSP procedures, *i.e.*, single-pass, two-pass, and three-pass, were used to process the Ti-35Nb-2Ta-3Zr β titanium alloy. During each pass, the sheet was cooled down in an argon atmosphere to prevent the sheet from oxidizing, and then the next FSP pass was performed with a 100 pct overlap in the same forward direction. In this work, the reference directions

LIQIANG WANG, Associate Professor, JIAO QU, Master Student, LIANGYU CHEN, Ph.D. Candidate, JINING QIN, Associate Professor, DI ZHANG, and WEIJIE LU, Professors, are with the State Key Laboratory of Metal Matrix Composites, Shanghai Jiao Tong University, Shanghai 200240, China. Contact e-mails: wang_liqiang@sjtu.edu.cn and luweijie@sjtu.edu.cn QIANG MENG, Engineer, is with the Beijing FSW Technology Co. Ltd, No. 1 Dongjunzhuang, Chaoyang District, Beijing 100024, China. LAI-CHANG ZHANG, Associate Professor, is with the School of Engineering, Edith Cowan University, 270 Joondalup Drive, Joondalup, Perth 6027, Australia.

Manuscript submitted March 3, 2015.
Article published online August 19, 2015

were selected as follows: ND, the rolling direction of the base material (*i.e.*, the transverse direction of the FSPed sample); RD, the normal direction; and TD, the original rotating direction. The specimens for microstructural examinations were cross-sectioned perpendicular to the ND. Microstructural observations were carried out by optical microscope (OM), transmission electron microscopy (TEM), and high-resolution transmission electron microscopy (HRTEM) with a JEM 2100 microscope operating at 200 kV, which can thus be used to estimate the area fraction of the phase transformation. Electron backscattered diffraction (EBSD) with a JSM-6700F scanning electron microscope (SEM) was used to clarify the details herein. Microhardness test was carried out on a 1600-6406 Micro-Vickers Hardness Tester primarily along the horizontal direction of the FSPed specimens. The maximum load was about 200 g, and a 30-seconds dwelling time was applied at the maximum load before unloading. The distance between individual indents was 0.5 mm.

Figure 1 shows the cross-sectional optical image of the Ti-35Nb-2Ta-3Zr obtained *via* single-pass processing at 375 rpm. Four distinct regions are distinctly observed: a basin-shaped stir zone (SZ), transition zone (TZ), heat-affected zone (HAZ), and base metal (BM). The cross-sectional image shows a basin-shaped stir zone which is in accordance with the investigation that lower tool rotation rate ranging from 300 to 500 rpm results in the generation of basin-shaped nugget zone.[22] Intense plastic deformation and frictional heating during FSP generate a recrystallized fine-grained microstructure within stirred zone, as shown in Figure 1(a). The SZ consists of homogeneous equiaxed β grains, which indicates that partial recrystallization occurs in the SZ. The TZ was subjected to both heating and deformation during FSP, which is characterized by a highly deformed structure (Figure 1(b)). HAZ experienced a thermal cycle, but did not undergo any plastic deformation. Massive lentoid laths with an average length of 40 μm is visible in the HAZ zone as shown in Figure 1(c). The BM (Figure 1(d)) is composed of a lot of coarse, equiaxed β grains with an average grain size of 65 μm.

Figure 2(a) shows the microstructure of the FSP sample obtained by EBSD mapping, and the corresponding grain size distribution is also indicated in Figure 2(b). The specimen exhibits relatively uniform microstructure with equiaxed grains and narrow grain size distribution. The average grain size is about 1.2 μm. Figure 2(c) shows the misorientation angle histogram, where the content of high-angle grain boundaries (HAGBs) is measured as 79 pct. Such high fraction of HAGBs implies that dynamic recrystallization (DRX) occurred during FSP. Such content of the HAGBs has also been reported in the SZ of FSPed/FSWed aluminum alloys.[22–24] Continuous absorption of dislocations on low-angle grain boundaries (LAGBs) results in the formation of HAGBs, which is consistent with the former report that dynamic recrystallization is related to relatively localized boundary migration usually occurring in high stacking fault energy (SFE) metals during large deformation at high temperature.[25] During FSP, the material undergoes substantial microstructural alteration, *i.e.*, crystallographic texture and various features of grain structure change significantly.[26] The inverse pole figures in Figure 2(d) reveal a weak texture, with a maximum below two times random. The result shows that the (001) plane is parallel to the ND direction which is also the transverse direction of the FSPed sample.

In order to further elucidate the deformation mechanism of the SZ at different passes, additional microstruc-

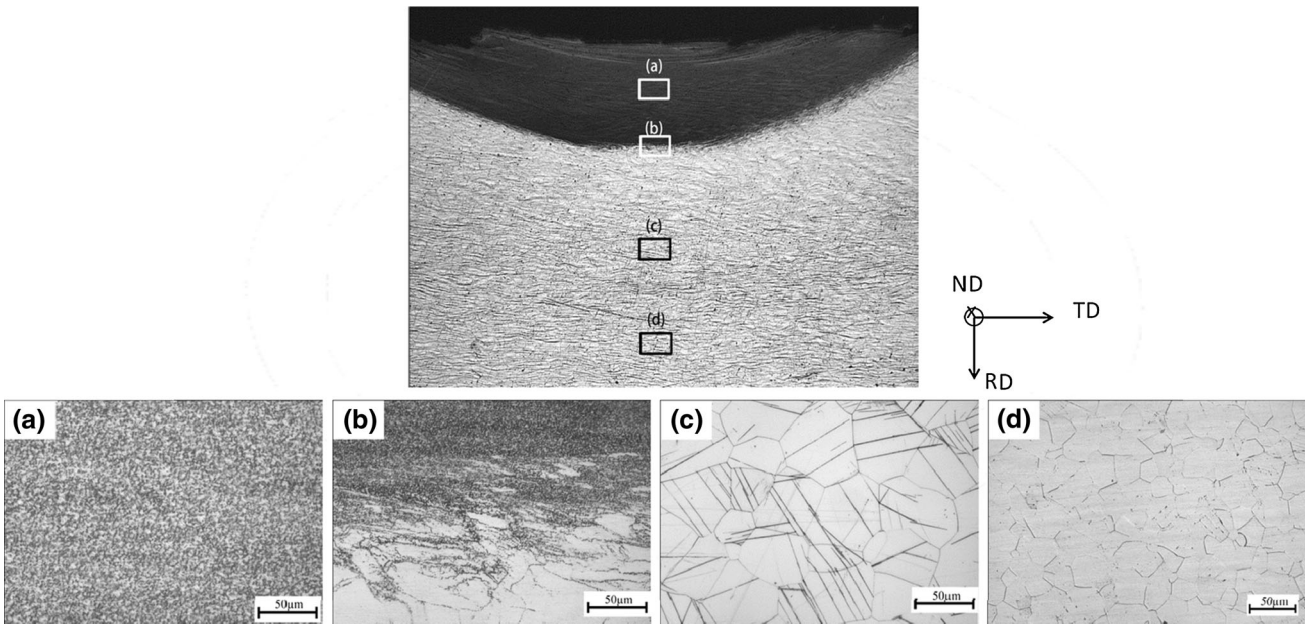

Fig. 1—Cross-sectional optical image of the single-pass friction-stir-processed Ti-35Nb-2Ta-3Zr sample and the magnified images of four distinct regions: (*a*) stir zone (SZ), (*b*) transition zone (TZ), (*c*) heat-affected zone (HAZ), and (*d*) base material (BM).

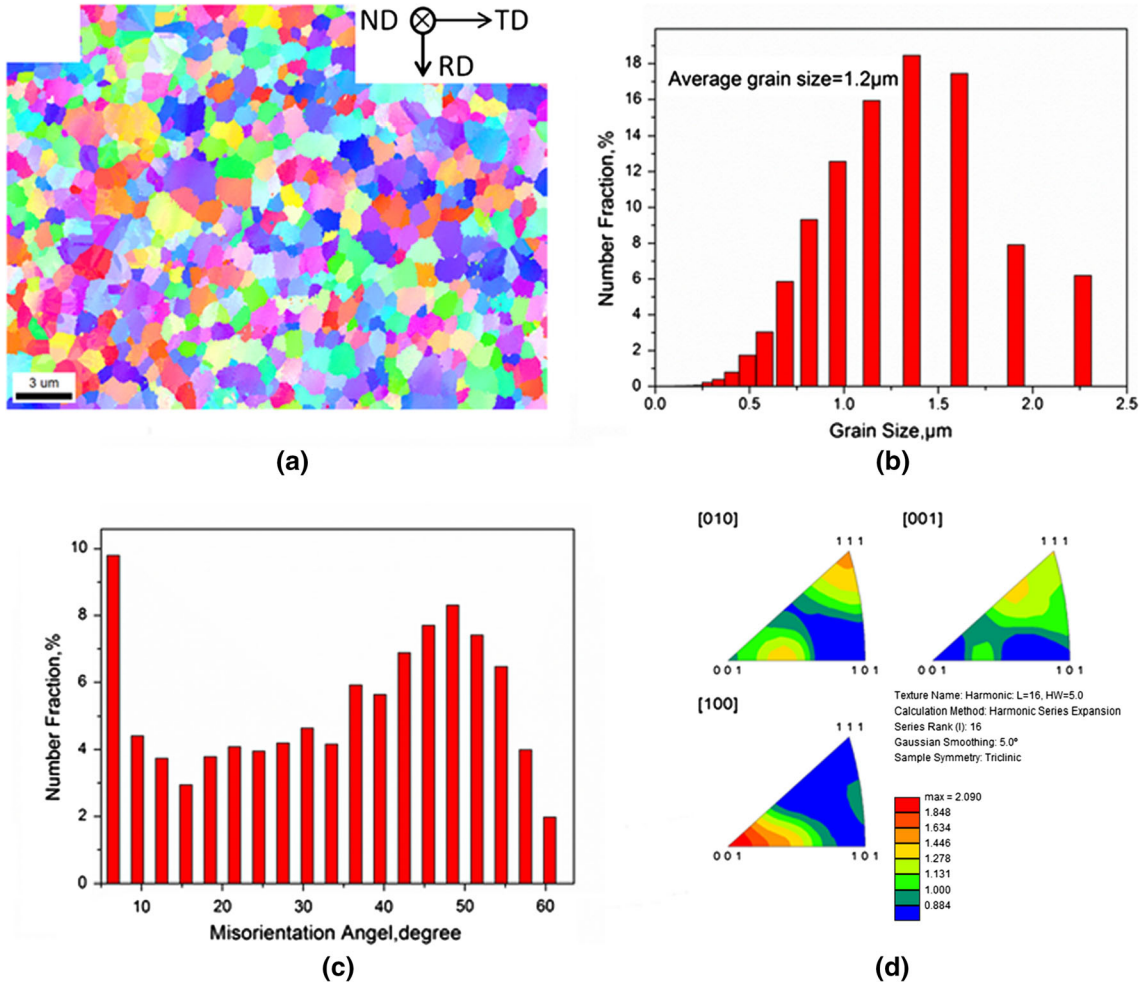

Fig. 2—EBSD maps of stir zone(SZ) in the single-pass Ti-35Nb-2Ta-3Zr FSP sample: (*a*) orientation map; (*b*) distribution of grain size; (*c*) boundary misorientation angle distribution; (*d*) TD{010}, ND{001}, RD{100} inverse pole figures.

tural information of SZ was investigated by TEM as shown in Figure 3. A typical β microstructure with an average grain sizes ranging from 1 to 2 μm is observed during single pass. Many dislocation tangles are presented in the grains, and dislocation walls are formed around the grain boundaries, as indicated by the black arrows in Figure 3(a), accompanying a small amount of α'' martensite precipitation. Acicular-shaped deformation-induced α'' martensite with a width of 20 nm is observed during single pass (Figure 3(b)). Further diffraction analysis reveals that nanosize ω phase is also induced, and the orientation relationship between β matrix and ω phase is $[011]_{\beta}//[11-20]_{\omega}$. At the initial stage (single-pass FSP) *via* severe plastic deformation, dislocations slipping and deformation-induced α'' phase accelerate the transformation of deformation-induced ω phase. This trend is supported by Figure 3(b), where ω phase is present, accompanying martensite which is clearly indicated by strong diffraction spots of ω phase.

After two passes, α'' martensite is precipitated around grain boundaries, which also clearly suggests that a large amount of dislocations dissolve instantaneously (Figure 3(c)). As shown in Figure 3(d), acicular α'' martensite becomes coarser to 50 to 60 nm in width. Compared with α'' phase appearing after first pass, such a difference in morphology could be explained by much more severe deformation which enhances the driving force for α'' martensites' nucleation and growth. Moreover, disperse ω phase in nanoscale is presented surrounding α'' martensite (Figure 3(b)) and also around plate-shaped deformation twins with a width of about 250 nm in the two-pass FSP sample (Figure 3(e)). The orientation relationship between α'' martensite and ω phase is $[001]\ \alpha''//[11-20]_{\omega}$. During this process, ω phase gradually disappeared as proved by the weaker diffraction spots of ω phase in Figure 3(e). Compared to the ω phase transformation before deformation twinning in the early stage of plasticity (first pass), nanosize ω phase would dissolve to β phase accompanied with dislocation annihilation, which was also observed in Ti-12Mo (wt pct) alloy.[27] It is reported that in metastable β titanium alloys, two kinds of deformed twins may exist: *i.e.*, $\{332\}_{\beta}\langle 113\rangle_{\beta}$ twins; and $\{112\}_{\beta}\ \langle 111\rangle_{\beta}$, which are related to the stability of quenched β phase.[28,29]

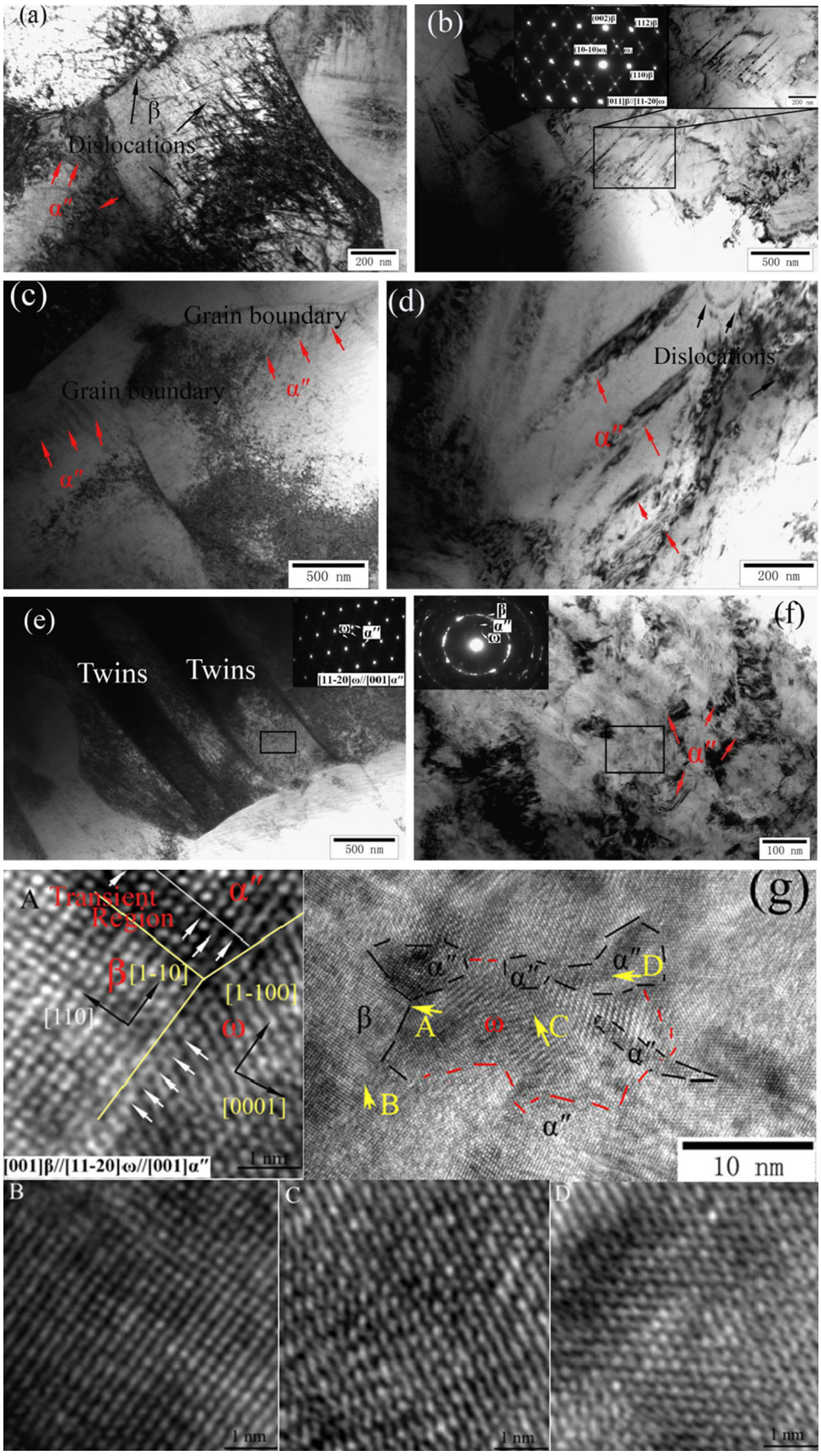
(a)
β
Dislocations
α″
200 nm
(b)
(002)β
(112)β
(10-10)α
ω
(110)β
(011)β//(11-20)α
500 nm
(c)
Grain boundary
Grain boundary
α″
α″
500 nm
(d)
Dislocations
α″
200 nm
(e)
Twins
Twins
ω
α″
[11-20]ω//[001]α″
500 nm
(f)
β
α′
ω
α″
100 nm
A Transient Region
α″
β[1-10]
[110]
[1-100]
ω
[0001]
[001]β//[11-20]ω//[001]α″
1 nm
(g)
α″
α″
α″
D
β
A
ω
C
α″
B
α″
10 nm
B
1 nm
C
1 nm
D
1 nm

◀Fig. 3—TEM micrographs of Ti-35Nb-2Ta-3Zr after (*a*) and (*b*) single-pass; (*c*), (*d*), and (*e*) two-pass; (*f*) and (*g*) three-pass FSP: (a) small β grains around 1 μm in size with many dislocation tangles inside accompanying with α'' martensite precipitation, (b) α'' martensite about 20-nm width and SAED pattern, (c) α'' martensite precipitates around grain boundary with less dislocation inside β grains, (d) relative coarse α'' martensite, (e) deformation twins and SAED pattern, (f) highly localized plastic deformation regions with ultrafine grains and the corresponding SAED pattern, and (g) HRTEM image of enlarged domain of marked black box (f) with β, α'', and ω phase particles.

Figure 3(f) shows the TEM image of the three-pass sample, where the grains are greatly refined to the nanoscale, and the grain boundaries are invisible. Compared with the two-pass specimen, in the three-pass specimen, plate-shaped deformation twins almost disappear, instead of nanosized β phase and deformation-induced martensite. This shows that dislocation motion together with martensite precipitation dominate the grain refinement in FSP. Meanwhile, deformation-induced ω particles precipitate around martensite and deformation twins also accelerate grain refinement and contribute to further plastic deformation, which is similar to the results in (Reference 30).

Figure 3(g) shows the HRTEM image of the enlarged domain of marked black box in Figure 3(f), focusing mainly on the phase transformation about β, α'', and ω particles. The incident beam is along the [001] direction of the β matrix. Four enlarged individual areas named by A, B, C, and D represent the bonding point of β, α'', and ω phase, β phase, ω phase, and α'', respectively. There is no sharp boundary between β and ω phases because of the structural similarity and coherent nature of the interface. As seen from the transient region between β and α'' in domain A (Figure 3(g)), a severely distorted β crystal in this region showing stretched distortions along $[1\bar{1}0]_\beta$ direction results likely from stacking fault and dislocation during deformation, which would accelerate the transformation from β to α''. This is also good evidence that α'' is present accompanying with dislocation annihilation, as discussed above. While for the interface between β and ω, atoms are arranged in dense with a coherent interface. Some compressive distortion along $[0001]_\omega$ direction can be detected, which to the contrary promotes the transformation from ω to β. Similar to the phenomenon discussed above, the amount of ω phase is reduced with the increasing pass number, suggesting that the reverse transformation from ω to β has taken place. According to Wang *et al.*'s report,[31] the reverse ω to β transformation is grain-size dependent and ω phase to β phase transformation occurs when the grain size is less than 100 nm. This reversible ω to β phase transformation phenomenon is also observed in Ti-36Nb-2.2Ta-3.7Zr-0.3O alloy,[10] and the de-twinning process of deformation twins were also reported in (Reference 32). The reversible ω to β phase transformation is also accompanied with α'' phase during FSP in the present paper. The amount of deformation-induced ω phase decreases gradually with the increase in pass number, especially in the three-pass specimen. However, different from the results in (Reference 31), selected area electron diffraction (SAED) pattern (Figure 3(f) also indicates ω phase in the condition that the matrix grain is refined to nanometer. In the overlapped regions after two passes, much more stable recrystallized ultrafine grain structures would prevent deformation twin. Thus, finer acicular α'' martensite can only be induced after three passes. Based on our investigation, ω phase transformation will benefit much from the nanosize α'' phase though some reverse transformation from ω phase to β phase occurs.

Figure 4 indicates the effect of different FSP parameters on the microhardness of Ti-35Nb-2Ta-3Zr alloy along the horizontal direction, when the rotating speed is 375 rpm. Compared with the microhardness (189 Hv) in base material, an increase in deformation pass from single pass to three passes increases the average microhardness values in stir zone from 208 to 231 Hv and 247 Hv, respectively. Tiny dispersions of α'' martensite together with reduced grain in nanometer level eventu-

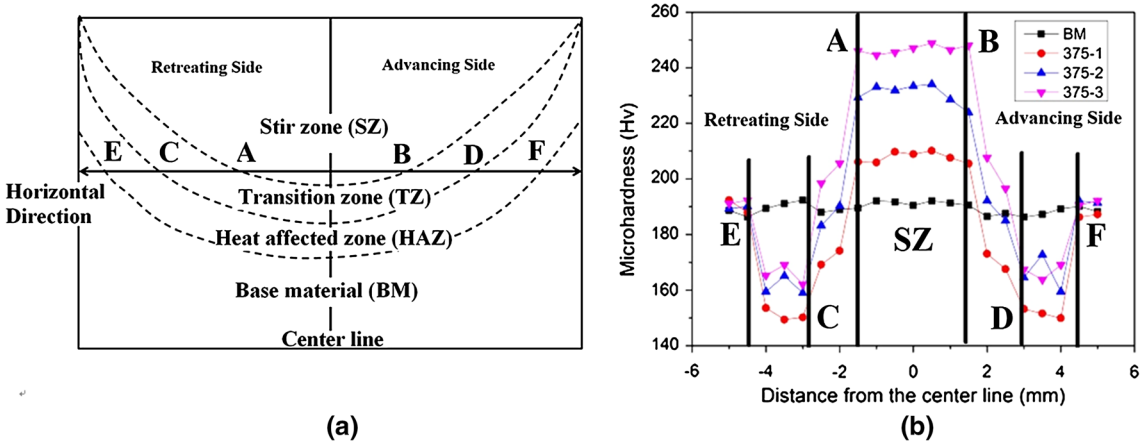

Fig. 4—Effect of different friction-stir processing parameters on the microhardness of Ti-35Nb-2Ta-3Zr alloy: (*a*) Schematic diagram of the testing direction along horizontal direction; (*b*) Microhardness values of different processing passes.

ally enhance the microhardness values. However, coarser grain size in both transition zone (TZ) and heat-affected zone (HAZ), as indicated in Figure 1, would decrease the microhardness.

In summary, complex deformation mechanisms are found in FSPed Ti-35Nb-2Ta-3Zr alloy. During FSP, at the initial stage, accompanying deformation-induced ω phase, the dominant deformation mechanisms include dislocation slipping, deformation-induced α'' martensite phase transformation and deformation twinning. With an increase in friction stir passes, α'' phase is coarsened, and the deformation twin disappears. A reverse deformation-induced ω to β transformation and de-twinning process are observed along with the refined grains to the nanoscale, and compressive distortions along [0001]ω direction promotes the transformation from ω to β. Tiny dispersions of α'' martensite together with reduced grain size to the nanometer scale eventually enhance the microhardness values in stir zone, especially for the FSPed specimen after three passes.

We would like to acknowledge the financial support provided by the National Science Foundation under Grant No: 51302168, 81171738, 973 Program under Grant No: 2014CB046701., Shanghai Natural Science Foundation under Grant No: 12ZR1445500, New Teachers' Fund for Doctor Stations, Ministry of Education under Grant No: 20120073120007, and under the Australian Research Council's Projects funding scheme (DP110101653).

REFERENCES

1. T. Saito, T. Furuta, J.H. Hwang, S. Kuramoto, K. Nishino, N. Suzuki *et al.*: *Science*, 2003, vol. 300, pp. 464–67.
2. E. Withey, M. Jin, A. Minor, S. Kuramoto, D.C. Chrzan, and J.W. Morris: *Mater. Sci. Eng. A*., 2008, vol. 493, pp. 26–32.
3. E.A. Withey, A.M. Minor, D.C. Chrzan, J.W. Morris, Jr, and S. Kuramoto: *Acta Mater*., 2010, vol. 58, pp. 2652–65.
4. X. Tang, T. Ahmed, and H. Rack: *J. Mater. Sci*., 2000, vol. 35, pp. 1805–11.
5. L. Elias, S. Schneider, S. Schneider, H. Silva, and F. Malvisi: *Mat. Sci. Eng. A*, 2006, vol. 432, pp. 108–12.
6. P.L. Ferrandini, F.F. Cardoso, S.A. Souza, C.R. Afonso, and R. Caram: *J. Alloy. Compd*., 2007, vol. 433, pp. 207–10.
7. Y. Hao, Z. Zhang, S. Li, and R. Yang: *Acta Mater*., 2012, vol. 60, pp. 2169–77.
8. L. Wang, W. Lu, J. Qin, F. Zhang, and D. Zhang: *Mat. Sci. Eng. A*, 2008, vol. 490, pp. 421–26.
9. Y. Xu, D. Yi, H. Liu, X. Wu, B. Wang, and F. Yang: *Mater. Sci. Eng. A*, 2012, vol. 547, pp. 64–71.
10. Y. Wang, Y. Zhao, Q. Lian, X. Liao, R. Valiev, S. Ringer, Y. Zhu, and E. Lavernia: *Scripta Mater*., 2010, vol. 63, pp. 613–16.
11. Y. Ivanisenko, I. MacLaren, X. Sauvage, R. Valiev, and H.-J. Fecht: *Acta Mater*., 2006, vol. 54, pp. 1659–69.
12. T. Waitz, V. Kazykhanov, and H. Karnthaler: *Acta Mater*., 2004, vol. 52, pp. 137–47.
13. D. Alloyeau, C. Ricolleau, C. Mottet, T. Oikawa, C. Langlois, Y. Le Bouar, N. Braidy, and A. Loiseau: *Nat Mater*., 2009, vol. 8, pp. 940–46.
14. D. Hughes and N. Hansen: *Acta Mater*., 1997, vol. 45, pp. 3871–86.
15. J. Huang, Y. Zhu, H. Jiang, and T. Lowe: *Acta Mater*., 2001, vol. 49, pp. 1497–05.
16. N. Tao and K. Lu: *Scripta Mater*., 2009, vol. 60, pp. 1039–43.
17. W. Xu, X. Wu, D. Sadedin, G. Wellwood, and K. Xia: *Appl. Phys. Lett*., 2008, vol. 92, p. 011924.
18. H. Nakayama, K. Tsuchiya, and M. Umemoto: *Scripta Mater*., 2001, vol. 44, pp. 1781–85.
19. K. Tsuchiya, M. Inuzuka, D. Tomus, A. Hosokawa, H. Nakayama, K. Morii, Y. Todaka, and M. Umemoto: *Mater. Sci. Eng. A*, 2006, vol. 438, pp. 643–48.
20. Q. Li, M. Niinomi, J. Hieda, M. Nakai, and K. Cho: *Acta Biomater*., 2013, vol. 9, pp. 8027–35.
21. Z. Ma, A. Pilchak, M. Juhas, and J. Williams: *Scripta Mater*., 2008, vol. 58, pp. 361–66.
22. R.S. Mishra and Z. Ma: *Mater. Sci. Eng. R*, 2005, vol. 50, pp. 1–78.
23. F.C. Liu, P. Xue, Z.Y. Ma, and J. Mater: *Sci. Technol*., 2012, vol. 28, pp. 1025–30.
24. A. Gerlich and T. Shibayanagi: *Scripta Mater*., 2009, vol. 60, pp. 236–39.
25. L. Wu, D. Wang, B. Xiao, and Z. Ma: *Scripta Mater*., 2014, vols. 78–79, pp. 17–20.
26. J.H. Cho and P.R. Dawson: *Metall. Mater. Trans. A*., 2006, vol. 37A, pp. 1147–64.
27. F. Sun, J.Y. Zhang, M. Marteleur, T. Gloriant, P. Vermaut, D. Laille, P. Castany, C. Curfs, P.J. Jacques, and F. Prima: *Acta Mater*., 2013, vol. 61, pp. 6406–17.
28. S. Hanada and O. Izumi: *Metall. Trans. A*., 1987, vol. 18, pp. 265–71.
29. N. Sakaguchi, M. Niinomi, and T. Akahori: *Mater. Trans*., 2004, vol. 45, pp. 1113–19.
30. H. Liu, M. Niinomi, M. Nakai, J. Hieda, and K. Cho: *Scripta Mater*., 2014, vol. 82, pp. 29–32.
31. Y.B. Wang, Y.H. Zhao, Q. Lian, X.Z. Liao, R.Z. Valiev, S.P. Ringer, Y.T. Zhu, and E.J. Lavernia: *Scripta Mater*., 2010, vol. 63, pp. 613–16.
32. L. Qu, Y. Yang, Y. Lu, L. Feng, J. Ju, P. Ge, W. Zhou, D. Han, and D. Ping: *Scripta Mater*., 2013, vol. 69, pp. 389–92.